Altered regulation of mesenchymal cell senescence promotes pathological changes associated with diabetic wound healing

Arisa Kita
Sapporo Medical University
Yuki Saito
Sapporo Medical University School of Medicine https://orcid.org/0000-0002-7949-1628
Miura Norihiro
Hokkaido University
Maki Miyajima
Hokkaido University
Takatoshi Yotsuyanagi
Sapporo Medical University
Mineko Fujimiya
Sapporo Medical University
Takako Chikenji (chikenji@pop.med.hokudai.ac.jp)
Hokkaido University https://orcid.org/0000-0003-2832-3656

Article

Keywords: senescence, wound healing, diabetes, SASP, mesenchymal cell

Posted Date: June 3rd, 2021

DOI: https://doi.org/10.21203/rs.3.rs-568349/v1

Version of Record: A version of this preprint was published at Communications Biology on April 5th, 2022. See the published version at https://doi.org/10.1038/s42003-022-03266-3.

Abstract

Pathologic diabetic wound healing is caused by sequential and progressive deterioration of hemostasis, inflammation, proliferation, and resolution/remodeling. Cellular senescence promotes physiological wound process; however, diabetic wounds exhibit low levels of senescent factors and accumulate senescent cells, which impair the healing process. In this study, we demonstrate that the number of $p15^{INK4B}$ + senescent PDGFR-α + mesenchymal cells in adipose tissue transiently increases in early phases of wound healing in non-diabetic mice and humans. Transplantation of adipose tissue from diabetic mice into non-diabetic mice results in wound healing impairment and an alteration in the cellular senescence-associated secretory phenotype (SASP), suggesting that insufficient induction of adipose tissue senescence after injury is a pathological mechanism of diabetic wound healing. These results give novel insight into how regulation of senescence in adipose tissue contributes to the wound healing process and provide the basis for the development of therapeutic approaches for wound healing impairment in diabetes.

Introduction

Cellular senescence is a process in which cells cease dividing, and it is activated in response to numerous stressors, including exposure to genotoxic agents, nutrient deprivation, hypoxia, mitochondrial dysfunction, and oncogene activation[1]. One of the features of senescent cells is that they undergo distinctive phenotypic alterations called the senescence-associated secretory phenotype (SASP), wherein they secrete cytokines, chemokines, growth factors, and matrix metalloproteases (MMPs)[1–3]. Senescent cells exert beneficial or detrimental effects on both tissue remodeling and dysfunction through cell-to-cell communication and SASP expression[2,3]. Beneficial effects of senescence include tissue remodeling and regeneration. Increased senescent cells are observed in the human skin during normal wound healing, heart regeneration in zebrafish and neonatal mice, and tissue regeneration in salamanders and zebrafish[4–7]. By contrast, chronically accumulated senescent cells exhibit an anti-apoptotic phenotype and a SASP, which induce detrimental effects including lung fibrosis, kidney and heart dysfunction, impairment of the central neuronal system, and muscle weakness[8].

In normal wound healing, the levels of senescent fibroblasts and endothelial cells are increased in the skin, and wound closure is accelerated by the induction of myofibroblast differentiation through the secretion of platelet-derived growth factor (PDGF) AA[9]. Senescent fibroblasts in skin wounds are also induced by cellular communication network factor 1 (CCN1) or CCN2, which inhibit excess fibrosis[10,11]. By contrast, increased senescent fibroblasts in diabetic wounds produce high levels of matrix-degrading proteases and inflammatory cytokines, resulting in healing impairment[12–14]. When greater than 15% of cells isolated from diabetic ulcers are senescent fibroblasts, a delay in wound healing is observed[15]. However, the regulatory mechanisms that govern these properties of cell senescence, specifically concerning their contribution to modifying tissue homeostasis and pathological conditions by producing various cytokines and growth factors, remain unknown.

Adipose tissue is attracting attention for promoting wound healing[16–20]. Within subcutaneous adipose tissue, stromal vascular cells and their subsets release growth factors and cytokines critical for neovascularization and wound repair[20]. Subcutaneous tissue has garnered attention particularly in obesity and type-2 diabetes because increased inflammation can alter the outcome of wound repair through the production of large numbers of hormones and cytokines, such as tumor necrosis factor α (TNF-α), Interleukin 6 (IL-6), and plasminogen activator inhibitor 1 (PAI-1)[21]; these proteins are the major components of the SASP. Senescent cell accumulation in the adipose tissue of patients with diabetes and obesity is associated with insulin resistance and systemic inflammation[22–26]. Furthermore, subcutaneous adipose tissue in obese subjects is characterized by an excessive amount of interstitial fibrosis and phenotypic changes in human pre-adipocytes, which may contribute to tissue deterioration[27].

In this study, we investigated cellular senescence in skin and subcutaneous adipose tissue during the wound healing process using a *Lepr*$^{db/db}$ type-2 diabetic mouse model. We found that growth of subcutaneous adipose tissue reached the wound site in control mice; however, in the diabetic *Lepr*$^{db/db}$ mice, the adipose tissue remained below the granulating tissue, and thereby impaired wound healing. In addition, transplantation of *Lepr*$^{db/db}$-derived adipose tissue into control mice impaired wound healing. In the adipose tissue of control mice, senescent cells increased at 2 days post-wound (DPW) and decreased at 8 DPW, whereas senescent cells in *Lepr*$^{db/db}$ mice remained low at 2 DPW and increased slightly at 8 DPW. The composition of the SASP factors differ between the control and *Lepr*$^{db/db}$ mice, resulting in the inhibition of fibroblast migration. Our results demonstrate that diabetic adipose tissue impairs transient senescence during pathological healing, which causes deteriorated wound healing, suggesting that cellular senesces of adipose tissue could be a therapeutic target for diabetic ulcers.

Results

Type-2 diabetic mice models have impaired wound healing

C57BLKS/J Iar -Lepr^{db}/+Lepr^{db} (*Lepr*$^{db/db}$) and C57BLKS/J Iar -m+/+Lepr^{db} (*Lepr*$^{db/+}$) mice were used in this study as type-2 diabetic and control mouse models, respectively. Blood glucose level ≤ 200 mg/dL (*Lepr*$^{db/+}$) or > 300 mg/dL (type-2 diabetic, *Lepr*$^{db/db}$) was used to confirm the absence or presence of diabetes, respectively (Fig. 1a). Full-thickness excisional skin wounds were created on the backs of *Lepr*$^{db/db}$ and *Lepr*$^{db/+}$ mice, and the wound closure rate was evaluated at 2 DPW, 5 DPW, and 8 DPW. At each time-point, the wound closure rates were impaired to a greater extent in *Lepr*$^{db/db}$ mice than in *Lepr*$^{db/+}$ mice (Fig. 1b and 1c). Histological analysis, using hematoxylin and eosin (H&E) and Masson trichrome stain, indicated that adipose tissues were present immediately under the wound eschar region in *Lepr*$^{db/+}$ mice at 2 DPW; however, in *Lepr*$^{db/db}$ mice, cell infiltration with collagen deposition was observed under the wound eschar region (Fig. 1d). At 8 DPW in *Lepr*$^{db/+}$ mice, the adipose tissue under the wound eschar decreased with wound closure. By contrast, in *Lepr*$^{db/db}$ mice, increased cell infiltration with collagen deposition was beneath the wound eschar region, and the adipose tissues were observed

under cell infiltration with collagen deposition at the wound closing region (Fig. 1d). Next, we used platelet-derived growth factor receptor α (PDGFR-α) and α smooth muscle actin (α-SMA) antibodies to identify mesenchymal stromal cells that produce ECM and play important roles in wound healing of subcutaneous tissue of the skin[28]. PDGFR-α is a cell surface receptor tyrosine kinase expressed in mesenchymal stromal cells in a variety of tissues and is also used as a marker for adipose progenitor cells [29–32]. Immunohistochemical analysis indicated that PDGFR-α–positive cells were located along the panniculus carnosus layer in the wound region, and α-SMA–positive cells were located on the panniculus carnosus layer at the wound edge in *Lepr*$^{db/+}$mice. However, *Lepr*$^{db/db}$ mice exhibited diffuse distribution of α-SMA– and PDGFR-α–positive cells on the wound region at 8 DPW (Fig. 1e).

Transplantation of adipose tissue derived from Lepr$^{db/db}$ mice into Lepr$^{db/+}$ mice impairs wound healing

To elucidate the role that adipose tissue plays in wound healing impairment, adipose tissue derived from *Lepr*$^{db/db}$ mice was transplanted into the excisional skin wound region of *Lepr*$^{db/+}$ mice. The excisional skin wound was sutured closed after transplantation to stabilize the transplanted tissue (Fig. 2a). We evaluated the histological wound healing score at 2 DPW and 8 DPW using H&E staining and Masson trichrome staining[33–35]. The histological wound healing scores in *Lepr*$^{db/db}$ adipose tissue transplanted mice (*Lepr*$^{db/db}$ ATT mice) were significantly lower than those for *Lepr*$^{db/+}$ adipose tissue transplanted mice (*Lepr*$^{db/+}$ ATT mice) (Fig. 2b and 2c). Immunohistochemical analysis indicated that *Lepr*$^{db/+}$ ATT mice had increased levels of PDGFR-α– and α-SMA–positive cells along the boundary line between the wound region and the normal dermis at 8 DPW (Fig. 2d). By contrast, *Lepr*$^{db/db}$ ATT mice had nonlocalized PDGFR-α– and α-SMA–positive cells at 8 DPW, which is also observed for impaired wound healing in *Lepr*$^{db/db}$ mice (Fig. 2d). These results suggest that transplantation of adipose tissue derived from *Lepr*$^{db/db}$ mice into *Lepr*$^{db/+}$ mice impairs wound healing.

To ascertain the role of cell movement in transplanted adipose tissue, we investigated the localization of CM-DiI–labeled adipose tissue–derived cells in wound regions. We identified CM-DiI–positive adipose cells in both the *Lepr*$^{db/+}$ ATT and *Lepr*$^{db/db}$ ATT mice in layers below the panniculus carnosus layer at 2 DPW and 8 DPW, and the CM-DiI–positive cells remained under panniculus carnosus layer over time (Fig. 2e).

Senescence-related gene expression levels were transiently increased in subcutaneous adipose tissue during wound healing

Senescent cells play beneficial roles in wound healing by expressing SASP factors including PDGF-AA, CCN1, VEGF, and Serpine1, which promote the production of ECM and prevent excessive fibrosis [9]. By contrast, accumulation of senescent cells is observed in diabetic ulcers[36]. We speculated that different types of cellular senescence occur between normal and diabetic wound healing in response to wounds. Hence, we investigated the time-dependent change in the expression of senescence-related factors during

wound healing in *Lepr*$^{db/db}$ and *Lepr*$^{db/+}$ mice. We harvested the skin and subcutaneous adipose tissue at pre-wound, 2 DPW, and 8 DPW. Skin and adipose tissue were divided by the panniculus carnosus layer.

In skin tissue, damage induced the expression of cellular senescence markers. *Cdkn1a* mRNA transcription levels increased at 8 DPW relative to those at pre-wound and 2 DPW in both *Lepr*$^{db/db}$ and *Lepr*$^{db/+}$ mice (Supplementary Fig. 1a). The *Trp53* transcription level decreased at 2 DPW relative to that of the pre-wound level in *Lepr*$^{db/+}$ mice, but the level in *Lepr*$^{db/db}$ mice was not significantly different (Supplementary Fig. 1a). *Cdkn2b* is a marker of cell senescence[37,38]. The transcription level of *Cdkn2b* mRNA increased at 2 DPW relative to that of the pre-wound level in *Lepr*$^{db/+}$ mice and decreased at 8 DPW relative to that of the level at 2 DPW in *Lepr*$^{db/db}$ mice (Supplementary Fig. 1a). The mRNA transcription level of the SASP-related factor *Serpine1* was essentially the same in both mouse models, but the *Serpine2* transcription level increased at 8 DPW in *Lepr*$^{db/db}$ mice (Supplementary Fig. 1a).

Next, we investigated the mRNA levels in subcutaneous adipose tissue during wound healing. The mRNA transcription levels of *Cdkn2b* and *Trp53* in *Lepr*$^{db/+}$ mice increased at 2 DPW relative to those at pre-wound, and the level of *Cdkn2b* transcription decreased at 8 DPW (Fig. 3a). In *Lepr*$^{db/db}$ mice, *Cdkn2b* and *Trp53* transcription levels did not significantly change during wound repair, and increased levels of *Cdkn1a*, *Serpine2*, and *Tgfb1* transcription, relative to 2 DPW, were observed at 8 DPW (Fig. 3a). The mRNA transcription levels of *Serpine1* and *Il6* did not change in *Lepr*$^{db/+}$ mice during wound healing, but *Lepr*$^{db/db}$ mice exhibited a time-dependent decrease in *Serpin1* and a transient increase in *Il6* levels (Fig. 3a). To clarify these differences in gene expression patterns related to senescence during the wound healing process between *Lepr*$^{db/+}$ and *Lepr*$^{db/db}$ adipose tissue, principal component analysis (PCA) was performed (Fig. 3b). The PCA plots indicate that *Lepr*$^{db/+}$ mice had large changes in senescence-related gene transcription at 2 DPW, whereas at 8 DPW, the transcription of these genes returned to a cluster similar to what was observed pre-wound. By contrast, *Lepr*$^{db/db}$ mice had minimal changes in senescence-related gene transcription during wound healing (Fig. 3b). To identify the cell type exhibiting senescence in subcutaneous adipose tissue, immunohistochemistry of p15^{INK4B}, which is encoded by *CDKN2B* and is an INK4 class of cell-cycle inhibitors[37,39], and PDGFR-α was performed. In *Lepr*$^{db/+}$ adipose tissue, the percentage of p15^{INK4B}+ in PDGFR-α+ cells increased at 2 DPW and 8 DPW, and the fluorescence intensity of p15^{INK4B} in PDGFRα+ cells transiently increased at 2 DPW (Fig. 3c and 3d). However, in *Lepr*$^{db/db}$ adipose tissue, an increase in the percentage of p15^{INK4B}+ in PDGFR-α+ cells was delayed at 8 DPW relative to that observed for *Lepr*$^{db/+}$ mice (Fig. 3c and 3d). In addition, the fluorescence intensity of p15^{INK4B} in PDGFR-α+ cells in *Lepr*$^{db/db}$ mice increased at 2 DPW but did not decrease at 8 DPW (Fig. 3c and 3d). These results suggest that cellular senescence rapidly occurs in *Lepr*$^{db/+}$ adipose tissue after wounding, and cell senescence is transient. However, in *Lepr*$^{db/db}$ adipose tissue, cell senescence is delayed after wounding, and this delay may allow for accumulation of senescent cells in diabetic wound healing.

Senescent PDGFR-α+ cells accumulate in subcutaneous adipose tissue during wound healing in diabetic patients

To test whether the number of senescent cells increases in subcutaneous adipose tissue during wound healing in diabetic or non-diabetic patients, we performed immunohistochemical analysis of PDGFR-α+ cells and looked for expression of $p15^{INK4B}$ and γH2A.X, which is a DNA damage-induced cell senescence marker[40]. Patient demographics are presented in Table 1. In non-diabetic patients, a negative correlation was observed between the percentage of $p15^{INK4B}$-positive cells in PDGFR-α–positive cells and the time post-wound (Fig. 4a and 4c). By contrast, in diabetic patients, we observed a high positive correlation between the percentage of PDGFR-α–positive cells that were $p15^{INK4B}$- or γH2A.X-positive and the time post-wound (Fig. 4b, 4c, and 4d). These results indicate that cell senescence gradually accumulates in diabetic adipose tissue during wound healing, but in non-diabetic patients, cell senescence occurs robustly in adipose tissue during the early stages of wound healing.

SASP factors derived from $Lepr^{db/db}$ mice adipose tissue impair wound healing

Overall, our results suggest that the difference in cell senescence between diabetic and non-diabetic adipose tissue influences wound healing. Because adipose-derived cells stayed under the panniculus carnosus layer during wound healing, SASP factors could be contributing to wound healing. Therefore, we evaluated the differences in the expression levels of SASP factors in $Lepr^{db/+}$ and $Lepr^{db/db}$ adipose tissue. Adipose tissue was collected from $Lepr^{db/+}$ and $Lepr^{db/db}$ mice at pre-wound, 2 DPW, and 8 DPW, and organ culture was performed to harvest SASP-containing culture media. A proteome profiler antibody array was used to investigate whether SASP factors were present in the culture media. At pre-wound, adipose tissue in $Lepr^{db/+}$ mice had higher expression levels of IGFBP3 and IGFBP5, but $Lepr^{db/db}$ mice have higher expression levels of CCL6 and CCL11. At 2 DPW, both $Lepr^{db/+}$ and $Lepr^{db/db}$ adipose tissue had increased expression levels of various secretory factors; however, the composition was different (Fig. 5a, 5b, and Supplementary Fig. 2). The $Lepr^{db/+}$ adipose tissue exhibited higher expression levels of Adiponectin, Ang2, CCL2, CRP, CXCL3, IL1Ra, MMP9, VEGF, and CCN4 (Fig. 5a, 5b, and Supplementary Fig. 2). By contrast, $Lepr^{db/db}$ adipose tissue had higher expression levels of IL11, CCL11, and MMP3 (Fig. 5a, 5b, and Supplementary Fig. 2). At 8 DPW, the levels of VEGF, IGFBP family members, and Serpin F1, which are important factors for wound healing [9,41], increased in $Lepr^{db/+}$ adipose tissue–derived conditioned media, but $Lepr^{db/db}$ conditioned media continued to have increased expression levels of CCL6, CCL11, and CXCL2 (Fig. 5a, 5b, and Supplementary Fig. 2). Finally, to test whether the conditioned media derived from $Lepr^{db/+}$ or $Lepr^{db/db}$ adipose tissue promotes or inhibits wound healing, we performed wound scratch assays that were treated with these conditioned media. We found that the conditioned media derived from $Lepr^{db/db}$ adipose tissue delays wound closure relative to the results from $Lepr^{db/+}$ adipose tissue (Fig. 5c and 5d).

Discussion

Cellular senescence contributes to wound healing in both the normal and pathological healing processes[9–15,42]. Therefore, it is critical to understand the role that cellular senescence plays in wound healing impairment, and modulating this senescence presents a novel therapeutic approach to reduce this impairment. In this study, we observed a rapid and transient increase in senescent cells in control adipose tissue; however, the number of senescent cells in diabetic *Lepr*$^{db/db}$ adipose tissue gradually increased post-wound. In normal wound healing, the number of senescent cells in mice skin increases 3–6 DPW and decreases 9 DPW, and genetic depletion of p16^{INK4A}-expressing senescent cells delays wound healing[9]. Senescent fibroblasts and endothelial cells in the dermis accelerate wound closure by inducing myofibroblast differentiation through the secretion of platelet-derived growth factor (PDGF) AA[9]. Our findings demonstrate the importance of transient cell senescence during wound healing, especially in adipose tissue.

In wound healing, dermal adipose tissue contributes to wound healing[19] and to the initiation of cutaneous fibrosis through adipocyte–myofibroblast transition[43]. We demonstrate that diabetic *Lepr*$^{db/db}$ mouse–derived adipose tissue transplantation into *Lepr*$^{db/+}$ impaired the wound healing process, even though the donor was normal dermal tissue. Furthermore, we found that the expression levels of SASP factors differ between *Lepr*$^{db/db}$- and diabetic *Lepr*$^{db/db}$-derived adipose tissue, which affects wound healing.

In the diabetic wound, VEGF and CCL2 enhance wound healing by promoting angiogenesis[20] and regulating macrophages[44], respectively. Secretion of VEGF increased at 2 DPW in adipose tissue from *Lepr*$^{db/+}$ mice but not in tissue from *Lepr*$^{db/db}$ mice. CCL2 secretion also increased at 2 DPW in adipose tissue in *Lepr*$^{db/+}$mice. The levels of CCN4, a regulator of senescence[45] that enhances wound healing by regulating dermal fibroblast cell migration, proliferation, and ECM expression[46], increased at 2 DPW in adipose tissue from *Lepr*$^{db/+}$mice. By contrast, diabetic *Lepr*$^{db/db}$ adipose tissue exhibited higher secretion of IL11, CCL11, and MMP3 at 2 DPW. IL11 is a member of the IL6 family of cytokines and binds to IL11 receptor subunit alpha (IL11RA), which is expressed on stromal cells and promotes tissue fibrosis[47,48]. In atopic dermatitis, the number of IL11-expressing cells is elevated in skin biopsy specimens relative to controls, and a significant correlation exists between IL11 and type I collagen deposition[49].

MMPs, known SASP factors[1], are important regulators of ECM degradation and deposition, and the timing and level of MMP activation are vital for determining whether successful wound healing or chronic non-healing is observed[50]. In normal wound healing, MMP9 expression increases concurrent with fibroblast migration into the wound area, and MMP3 levels increase at re-epithelialization[50]. In this study, the levels of MMP9 secretion increased in *Lepr*$^{db/+}$-derived adipose tissue at 2 DPW, and MMP3 levels increased at 8 DPW. However, in *Lepr*$^{db/d}$-derived adipose tissue, MMP3 increased at both 2 DPW and 8 DPW, suggesting that dysregulation of MMPs in adipose tissue results in wound healing impairment in *Lepr*$^{db/db}$ mice. Furthermore, the secretion levels of IGFBP3 and Serpin F1 in *Lepr*$^{db/+}$ adipose tissue

increased at 8 DPW. IGFBP3 is one of 6 structurally related IFGBPs that bind to IGF peptides with high affinity, and the IGFBP3•IGF1 complex binds to fibrin clots and concentrates at wound sites to facilitate wound healing[41]. Serpin F1 is a pigment epithelium–derived factor (PEDF), and PEDFs contribute to the resolution of wound healing by causing regression of immature blood vessels and stimulating maturation of the vascular microenvironment, which promotes a return to tissue homeostasis after injury[51]. Our findings suggest that *Lepr*$^{db/+}$ adipose tissue–secreted SASP factors promote wound healing by inducing cell migration and proliferation and inhibit fibrosis by inducing fibroblast senescence, which results in resolution of wound healing. By contrast, *Lepr*$^{db/db}$ adipose tissue–secreted SASP factors induce chronic inflammation, which results in wound healing impairment.

We identified a transient increase in p15^{INK4B}+ senescent PDGFR-α+ cells in adipose tissue during the normal wound healing process; however, in diabetic *Lepr*$^{db/db}$ mice, p15^{INK4B}+ senescent PDGFR-α+ cells steadily accumulated over the course of wound healing. Accumulation of p15^{INK4B}+ senescent PDGFR-α+ cells is also observed in diabetic patients, and non-diabetic patients have a decreased number of senescent cells during wound healing. PDGFR-α+ mesenchymal stromal cells in skeletal muscle exhibit transient senescence, and this promotes muscle regeneration after acute muscle injury[52,53]. PDGFR-α+ or vimentin+ cells in neonatal hearts exhibit transient senescence to promote regeneration[6,7]. Using PCR and immunohistochemical analysis, we found that the levels of p15^{INK4B}, encoded by the *Cdkn2b* gene, significantly increased in *Lepr*$^{db/+}$ adipose tissue at 2 DPW. CDKN2B expression levels are highest in subcutaneous adipose tissue relative to other tissues such as bone marrow, the central nervous system, skeletal muscle, and the internal organs[54]. Furthermore, CDKN2B expression levels in subcutaneous adipose tissue are correlated with BMI[54].

Although the detailed function of p15^{INK4B} is not as well understood as those for p16^{INK4A} and other senescence-related factors[55], the function and protein structure of p15^{INK4B} are predicted to be similar to p16^{INK4A}, and p15^{INK4B} is upregulated in TGF-β–related cell senescence [56]. p15^{INK4B} binds to CDK4 and CDK6, preventing their binding to cyclins and thereby inhibiting cell cycle progression[56]. The antiproliferative action of TGF-β is also mediated through the inhibition of c-Myc expression. c-Myc inhibits the expression of p15^{INK4B} and p21^{Cip1} in proliferating cells[57], and suppression of c-Myc by TGF-β limits c-Myc availability and suppresses the activity of p15^{INK4B} and p21^{Cip1}[58,59]. TGF-β expression and activation are rapidly induced in response to injury, and TGF-β controls wound healing by acting as a potent chemoattractant for monocytes and fibroblasts[60]. Although the role of TGF-β in the control of diabetic wound healing remains to be fully explained, increased levels of TGF-β1 are linked with type-2 diabetes, and TGF-β1 contributes to diabetic wound healing[61]. The regulation of TGF-β–related cell senescence may be a therapeutic target for diabetic ulcers.

Our intriguing results suggest that the transient increase in the number of senescent PDGFR-α+ cells in adipose tissue is important for wound healing, and that diabetic wounds exhibit a decrease in cell senescence in the acute wound-healing phase that results in impairment of wound healing concurrent

with accumulation of senescent cells. However, the study had several limitations. We analyzed subcutaneous adipose tissue; however, intradermal adipose tissue contributes to wound healing through regulation of adipocyte precursor proliferation and mature intradermal adipocyte repopulation in the skin after wounding[19]. The anatomical location of intradermal adipose tissue and subcutaneous adipose tissue is separated by the panniculus carnosus in mice, but human skin does not have a detectable panniculus carnosus. It is also difficult to confirm the existence of intradermal adipose tissue in humans because of the obvious inability to conduct lineage-tracing studies[62,63]. Even though intradermal and subcutaneous adipose tissue are not physically demarcated in humans, increasing evidence suggests that there is a functional distinction between these tissues[63]. Hence, careful interpretation of our results is needed, but at a minimum, we have demonstrated that cellular senescence in subcutaneous adipose tissue contributes to both normal and diabetic wound healing. Next, our study focused on PDGFR-a+ mesenchymal cell senescence in adipose tissue. Macrophages are one of the senescent cell populations in the diabetic wound[36], and their abundance is correlated with senescent cell burden in adipose tissue[23–26]. Although PDGFR-a+ cells play important roles in adipose tissue homeostasis[64], further study is needed regarding the role that macrophage senescence plays in adipose tissue during wound healing. Finally, we used the *Lepr*$^{db/db}$ diabetic mouse model, which is widely used as a typical delayed healing model[65], and our findings are similar to what is observed in type-2 diabetic patients. To better understand adipose tissue–related mechanisms in diabetic wound healing, further study is needed using a type-1 diabetic model, which exhibits adipose tissue atrophy and fibrosis[66–68]. In summary, we demonstrate that transient mesenchymal cell senescence occurs in adipose tissue in physiological wound healing; however, accumulation of cell senescence occurs concurrently with expression of different components of the SASP in diabetic wound healing, suggesting that impairment of senescence in adipose tissue contributes to intractable wound healing in diabetes.

Methods

Human wound samples

Six wound tissue samples from five diabetic patients (age: 68.7±9.0 years old; HbA1c(NGSP): 7.02±2.15%) and six wound tissue samples from six non-diabetic patients (age: 58.0±21.7 years old) were used in the study. The tissues used in the study were debrided and disposed during surgery for treatment, and no additional excisions were made for the study. Samples were recruited after agreement was obtained through informed consent. Detailed information about these subjects is given in Table 1. The Ethical Review Board at the Sapporo Medical University in Japan approved the study.

Animals

The Committee of the Animal Experimentation Center at the Sapporo Medical University School of Medicine approved all animal protocols. Mice were fed a standard chow diet and were maintained on a 12 h light / 12 h dark cycle with free access to food and water at all times. Male C57BLKS/JIar-

+Lepr^{db}/+Lepr^{db} (*Lepr$^{db/db}$*), male C57BLKS/JIar-m+/+Lepr^{db} (*Lepr$^{db/+}$*), and female C57BL/6 mice (age>11 weeks; Sankyo Lab Service, Tokyo, Japan) were used in the experiments. At 10–11 weeks of age, blood samples were taken from the tail to measure blood glucose, which was confirmed to be above 300 mg/dL in the diabetic mice and below 200 mg/dL in the control mice. Nipro Stat Strip XP2 (Nova Biomedical, Tokyo, Japan) was used for blood glucose level measurements.

Wound model

Mice were anesthetized using mixed anesthetic agents (medetomidine, midazolam, butorphanol)[69]. To create the skin ulcer model, a 10 mm diameter, full-thickness circle excision was made on the back of *Lepr$^{db/db}$* and *Lepr$^{db/+}$* mice. Wounds were photographed with a digital camera (COLPIX S9700; Nikon, Tokyo, Japan). Images were analyzed by tracing the wound margin, and the enclosed pixel area was calculated using the Image J software, version 1.5 (National Institutes of Health, Bethesda, MD, USA). The wound areas were standardized by measuring the captured image. Using the original wound size for comparison, the percentage of wound closure was calculated as follows: day n area / day 0 area × 100 (%).

Adipose tissue transplantation

To perform adipose tissue transplantation, 100–120 mg of subcutaneous adipose tissue was collected from the back of *Lepr$^{db/db}$* and *Lepr$^{db/+}$* mice and labeled with Cell Tracker Vybrant CM-DiI Cell-Labeling Solution (V22888; Thermo Fisher Scientific, MA, USA). Labeling of adipose tissue was performed according to the protocol. Briefly, tissue was incubated with CM-DiI at 37°C for 5 minutes and at 4°C for 15 minutes. The labeled adipose tissue was transplanted onto the back of *Lepr$^{db/+}$* mice, and the wound was sutured with nylon thread.

Histological analysis and wound healing scoring

Wound tissue and adipose tissue were harvested with marginal skin and fixed in 4% paraformaldehyde at 4℃ overnight. The following day, the tissue was cut into 5 mm sections and was paraffin-embedded. Each slide was stained with H&E and Masson trichrome, which were used for histological wound-healing scoring. For the scoring, an examiner assesses the progression of wound healing on a 12-point scale for inflammation, granulation, and collagen deposition[33,35]. In brief, each sample was given a score from 1 to 12: 1–3, none to minimal cell accumulation and granulation tissue or epithelial migration; 4–6, thin, immature granulation tissue dominated by inflammatory cells but with few fibroblasts, capillaries, or collagen deposition and minimal epithelial migration; 7–9, moderately thick granulation tissue, dominated by inflammatory cells and more fibroblasts and collagen deposition; and 10–12, thick, vascular granulation tissue dominated by fibroblasts and extensive collagen deposition. Because the wound was sutured, epithelialization was excluded from the evaluation criteria. All images were captured using a BZ-X700 fluorescence microscope (KEYENCE, Osaka, Japan).

Immunofluorescence staining

Paraffin-embedded sections were deparaffinized and rehydrated for immunostaining. Antigen retrieval was performed in a microwave oven (95–98℃ for 10 minutes) using citrate buffer (10 mM sodium citrate, pH 6.0). After cooling, the slides were washed twice with deionized water and once with 1X Tris-buffered saline with Tween-20 (TBST) for 5 minutes each. The sections were blocked with 1% bovine serum albumin (BSA) in TBST for 15 minutes at room temperature (RT) and were then incubated with primary antibodies overnight at 4°C or for 1 hour at RT. After washing three times with TBST for 5 minutes each, the sections were incubated with SignalStain Boost IHC Detection Reagent (HRP, Rabbit #8114; Cell Signaling Technology, Danvers, MA, USA) for 30 minutes at RT in the dark. The sections were then washed in TBST three times for 5 minutes each and treated with TSA Plus Working Solution (Fluorescein, Cyanine 3, and Cyanine 5; AKOYA BIOSCIENCES, Malborough, MA, USA) for 10 minutes at RT in the dark. For multiplex staining, stripping was performed in a microwave oven (95–98℃ for 10 minutes) using citrate buffer. After cooling, staining with different tyramide fluorescent labels was performed according to the above procedure. Nuclei were labeled with Cellstain DAPI solution (1:1000, 4',6-diamidino-2-phenylindole; Dojindo, Kumamoto, Japan), and after further washes, the sections were mounted in VECTASHIELD (Vector Laboratories, Burlingame, CA, USA). The following primary antibodies were used: rabbit anti-p15 (1:500; ab53034; Abcam, Cambridge, UK), rabbit anti–PDGFR-a (1:1000 (mouse) and 1:500 (human); D1E1E, XP; Cell Signaling Technology), rabbit anti–a-SMA (1:500; D4K9N, XP; Cell Signaling Technology), and rabbit anti–phospho-histone H2A.X(Ser139) (1:480; Ser139, 20E3; Cell Signaling Technology). These primary antibodies were used after dilution with SignalStain Antibody Diluent (Cell Signaling Technology). All images were captured using a BZ-X700 fluorescence microscope (KEYENCE).

RNA extraction and quantitative real-time PCR

Total RNA was isolated from skin wound tissues and subcutaneous adipose tissues using TRI Reagent (Molecular Research Center, Cincinnati, OH, USA) and was reverse-transcribed into cDNA using the iScript cDNA Synthesis Kit (1708891; Bio-Rad). Quantitative real-time PCR was performed using SsoAdvanced Universal SYBR Green Supermix (Bio-Rad) in a 7500 Real-Time PCR System (Applied Biosystems, Foster City, CA, USA) with the following conditions: 95°C for 30 seconds and 40 amplification cycles of 95°C for 15 seconds and 60°C for 1 minute. Expression levels were normalized to glyceraldehyde 3-phosphate dehydrogenase (GAPDH) or beta-actin (ACTB) levels. The primer sequences used for the PCR analysis are shown in Supplementary Table 1.

Organ culture and SASP characterization

Subcutaneous adipose tissue under the wound for five *Lepr*$^{db/+}$ or *Lepr*$^{db/db}$ mice in each group [0 DPW (before wound), 2 DPW, and 8 DPW] was collected and put into phosphate-buffered saline (PBS) supplemented with 2% penicillin/streptomycin. The tissue was then washed and transferred to Dulbecco's Modified Eagle's Medium (DMEM) supplemented with 10% fetal bovine serum (FBS). The volume of the culture medium was 1 mL for every 60 mg of adipose tissue, the medium was changed once at 24 hours post-extraction, and the culture medium was collected at 48 hours post-extraction for use in the following

assay. The culture medium from adipose tissue culture was characterized using the Proteome Profiler Mouse XL Cytokine Array Kit (R&D Systems, Minneapolis, MN, USA). Developed films were imaged and integrated density analysis was performed using Image J, version 1.5 (National Institutes of Health).

Cell preparation and *in vitro* wound-healing assays

Skin fibroblasts were collected from C57BL/6 mice. After euthanasia, skin was harvested and digested in Liberase TL (5401020001, Merck) for 120 minutes at 37°C. The digested skin slurries were filtered through a 100 µm cell strainer (EASYstrainer Cell; Greiner Bio-One, Kremsmuenster, Austria) and through a 70 µm cell strainer (Greiner Bio-One). Cells were suspended in DMEM supplemented with 10% PBS and 1% penicillin/streptomycin and were cultured in a T75 culture flask. Cells reached 80–90% confluence after incubation for 1–2 weeks, and the cells were passaged. Cells from passage 2 were used for the *in vitro* studies. *In vitro* wound healing was studied using 2-well Culture-Inserts (Ibidi, Bavaria, Germany). Mouse skin–derived fibroblasts were cultured in 2-well Culture-Inserts with adipose tissue–cultured media for 6 days, and phase contrast images were obtained every 24 hours and immediately after removing the 2-well Culture-Insert using Primovert and Axiocam208 microscopes (Carl Zeiss, Jena, Germany).

Statistical analysis

Mice were only excluded from the study if they had visible wounds from fighting. Statistical analyses were performed using R (The R Foundation for Statistical Computing, Vienna, Austria). Statistical significance between two groups was determined using an unpaired t-test. A one-way or two-way analysis of variance (ANOVA) was conducted to assess differences among three or more groups. Pairwise comparisons were made only when the ANOVA test identified a statistical significance. *p*-values for multiple comparisons were adjusted using the Tukey method. Statistical analyses were performed using EZR, which is a graphical user interface for R[70]. Two-sided *p*-values <0.05 were considered statistically significant. Quantitative data are presented as either the mean±standard error of the mean (SEM) or median with interquartile range (IQR) and 1.5× IQR. Box-and-whisker plots and bar plots were generated using ggplot2, a plotting system for R based on The Grammar of Graphics (The R Foundation for Statistical Computing, Vienna, Austria). The R packages FactoMineR and factoextra were used to generate heat maps, Ward's hierarchical agglomerative clustering, and principal component analyses.

Declarations

Author contributions

AK, YS, and TSC designed the studies. AK, YS, TM, MM, and TSC performed the experiments and analyzed the data. AK, YS, MF, and TC contributed to drafting and reviewing the manuscript.

Acknowledgements

We would like to thank Tatsuya Shiraishi, Naoko Sai, and Yumiko Takagi for their technical support and Zenis for providing native language editing services. This work was supported by JSPS KAKENHI (Grant Number 19K18908) and LEOC.

Conflicts of interest

The authors declare no conflicts of interest.

Data availability

The data that support the findings of this study are available from the corresponding author upon reasonable request.

References

1. Gorgoulis, V. *et al.* Cellular Senescence: Defining a Path Forward. *Cell* **179**, 813–827 (2019).
2. Collado, M., Blasco, M. A. & Serrano, M. Cellular Senescence in Cancer and Aging. *Cell* **130**, 223–233 (2007).
3. Muñoz-Espín, D. & Serrano, M. Cellular senescence: from physiology to pathology. *Nat. Rev. Mol. Cell Biol.* **15**, 482–496 (2014).
4. Da Silva-Álvarez, S. *et al.* Cell senescence contributes to tissue regeneration in zebrafish. *Aging Cell* **19**, (2020).
5. Yun, M. H., Davaapil, H. & Brockes, J. P. Recurrent turnover of senescent cells during regeneration of a complex structure. *Elife* **4**, e05505-undefined (2015).
6. Sarig, R. *et al.* Transient p53-Mediated Regenerative Senescence in the Injured Heart. *Circulation* **139**, 2491–2494 (2019).
7. Feng, T. *et al.* CCN1-Induced Cellular Senescence Promotes Heart Regeneration. *Circulation* **139**, 2495–2498 (2019).
8. Paez-Ribes, M., González-Gualda, E., Doherty, G. J. & Muñoz-Espín, D. Targeting senescent cells in translational medicine. *EMBO Mol. Med.* **11**, e10234-n/a (2019).
9. Demaria, M. *et al.* An Essential Role for Senescent Cells in Optimal Wound Healing through Secretion of PDGF-AA. *Dev. Cell* **31**, 722–733 (2014).
10. Jun, J.-I. & Lau, L. F. The matricellular protein CCN1 induces fibroblast senescence and restricts fibrosis in cutaneous wound healing. *Nat. Cell Biol.* **12**, 676–685 (2010).
11. Jun, J.-I. & Lau, L. F. CCN2 induces cellular senescence in fibroblasts. *J. Cell Commun. Signal.* **11**, 15–23 (2017).
12. Mendez, M. V. *et al.* Fibroblasts cultured from venous ulcers display cellular characteristics of senescence. *J. Vasc. Surg.* **28**, 876–883 (1998).

13. Wilkinson, H. N. & Hardman, M. J. Wound senescence: A functional link between diabetes and ageing? *Exp. Dermatol.* **30**, 68–73 (2021).
14. Harding, K. G., Moore, K. & Phillips, T. J. Wound chronicity and fibroblast senescence - implications for treatment. *Int. Wound J.* **2**, 364–368 (2005).
15. Stanley, A. & Osler, T. Senescence and the healing rates of venous ulcers. *J. Vasc. Surg.* **33**, 1206–1211 (2001).
16. Correa-Gallegos, D. *et al.* Patch repair of deep wounds by mobilized fascia. *Nature* **576**, 287–292 (2019).
17. Kruglikov, I. L. & Scherer, P. E. Skin aging: are adipocytes the next target? *Aging (Albany. NY).* **8**, 1457–1469 (2016).
18. Festa, E. *et al.* Adipocyte Lineage Cells Contribute to the Skin Stem Cell Niche to Drive Hair Cycling. *Cell* **146**, 761–771 (2011).
19. Schmidt, B. A. & Horsley, V. Intradermal adipocytes mediate fibroblast recruitment during skin wound healing. *Development* **140**, 1517–1527 (2013).
20. Rodrigues, M., Kosaric, N., Bonham, C. A. & Gurtner, G. C. Wound Healing: A Cellular Perspective. *Physiol. Rev.* **99**, (2019).
21. Hajer, G. R., van Haeften, T. W. & Visseren, F. L. J. Adipose tissue dysfunction in obesity, diabetes, and vascular diseases. *Eur. Heart J.* **29**, 2959–2971 (2008).
22. Palmer, A. K., Gustafson, B., Kirkland, J. L. & Smith, U. Cellular senescence: at the nexus between ageing and diabetes. *Diabetologia* **62**, 1835–1841 (2019).
23. Kirkland, J. L., Hollenberg, C. H. & Gillon, W. S. Age, anatomic site, and the replication and differentiation of adipocyte precursors. *Am. J. Physiol. Physiol.* **258**, C206–C210 (1990).
24. Minamino, T. *et al.* A crucial role for adipose tissue p53 in the regulation of insulin resistance. *Nat. Med.* **15**, 1082–1087 (2009).
25. Tchkonia, T. *et al.* Fat tissue, aging, and cellular senescence. *Aging Cell* **9**, 667–684 (2010).
26. Palmer, A. K. *et al.* Targeting senescent cells alleviates obesity-induced metabolic dysfunction. *Aging Cell* **18**, e12950 (2019).
27. Henegar, C. *et al.* Adipose tissue transcriptomic signature highlights the pathological relevance of extracellular matrix in human obesity. *Genome Biol.* **9**, R14 (2008).
28. Werner, S., Krieg, T. & Smola, H. Keratinocyte–Fibroblast Interactions in Wound Healing. *J. Invest. Dermatol.* **127**, 998–1008 (2007).
29. Lemos, D. R. & Duffield, J. S. Tissue-resident mesenchymal stromal cells: Implications for tissue-specific antifibrotic therapies. *Sci. Transl. Med.* **10**, eaan5174-undefined (2018).
30. Cattaneo, P. *et al.* Parallel Lineage-Tracing Studies Establish Fibroblasts as the Prevailing In Vivo Adipocyte Progenitor. *Cell Rep.* **30**, 571-582.e2 (2020).
31. Berry, R. & Rodeheffer, M. S. Characterization of the adipocyte cellular lineage in vivo. *Nat. Cell Biol.* **15**, 302–308 (2013).

32. Shin, S. *et al.* Dynamic control of adipose tissue development and adult tissue homeostasis by platelet-derived growth factor receptor alpha. *Elife* **9**, (2020).
33. Greenhalgh, D. G., Sprugel, K. H., Murray, M. J. & Ross, R. PDGF and FGF stimulate wound healing in the genetically diabetic mouse. *Am. J. Pathol.* **136**, 1235–1246 (1990).
34. Nishimura, Y. *et al.* CXCR4 Antagonist AMD3100 Accelerates Impaired Wound Healing in Diabetic Mice. *J. Invest. Dermatol.* **132**, 711–720 (2012).
35. Maruyama, K. *et al.* Decreased Macrophage Number and Activation Lead to Reduced Lymphatic Vessel Formation and Contribute to Impaired Diabetic Wound Healing. *Am. J. Pathol.* **170**, 1178–1191 (2007).
36. Wilkinson, H. N. *et al.* Elevated Local Senescence in Diabetic Wound Healing Is Linked to Pathological Repair via CXCR2. *J. Invest. Dermatol.* **139**, 1171-1181.e6 (2019).
37. Sharpless, N. E. INK4a/ARF: A multifunctional tumor suppressor locus. *Mutat. Res. Mol. Mech. Mutagen.* **576**, 22–38 (2005).
38. Sharpless, N. E. & Sherr, C. J. Forging a signature of in vivo senescence. *Nat. Rev. Cancer* **15**, (2015).
39. Kim, W. Y. & Sharpless, N. E. The Regulation of INK4/ARF in Cancer and Aging. *Cell* **127**, 265–275 (2006).
40. González-Gualda, E., Baker, A. G., Fruk, L. & Muñoz-Espín, D. A guide to assessing cellular senescence *in vitro* and *in vivo*. *FEBS J.* **288**, (2021).
41. Campbell, P. G., Durham, S. K., Hayes, J. D., Suwanichkul, A. & Powell, D. R. Insulin-like Growth Factor-binding Protein-3 Binds Fibrinogen and Fibrin. *J. Biol. Chem.* **274**, 30215–30221 (1999).
42. Hiebert, P. *et al.* Nrf2-Mediated Fibroblast Reprogramming Drives Cellular Senescence by Targeting the Matrisome. *Dev. Cell* **46**, 145-161.e10 (2018).
43. Marangoni, R. G. *et al.* Myofibroblasts in Murine Cutaneous Fibrosis Originate From Adiponectin-Positive Intradermal Progenitors. *Arthritis Rheumatol.* **67**, 1062–1073 (2015).
44. Wood, S. *et al.* Pro-Inflammatory Chemokine CCL2 (MCP-1) Promotes Healing in Diabetic Wounds by Restoring the Macrophage Response. *PLoS One* **9**, e91574 (2014).
45. Maiese, K. Picking a bone with WISP1 (CCN4): new strategies against degenerative joint disease. *J. Transl. Sci.* **2**, (2016).
46. Ono, M. *et al.* CCN4/WISP1 controls cutaneous wound healing by modulating proliferation, migration and ECM expression in dermal fibroblasts via α5β1 and TNFα. *Matrix Biol.* **68–69**, 533–546 (2018).
47. Ng, B. *et al.* Fibroblast-specific IL11 signaling drives chronic inflammation in murine fibrotic lung disease. *FASEB J.* **34**, 11802–11815 (2020).
48. Schafer, S. *et al.* IL-11 is a crucial determinant of cardiovascular fibrosis. *Nature* **552**, 110–115 (2017).
49. Toda, M. *et al.* Polarized in vivo expression of IL-11 and IL-17 between acute and chronic skin lesions. *J. Allergy Clin. Immunol.* **111**, 875–881 (2003).

50. Caley, M. P., Martins, V. L. C. & O'Toole, E. A. Metalloproteinases and Wound Healing. *Adv. Wound Care* **4**, 225–234 (2015).
51. Wietecha, M. S. *et al.* Pigment epithelium-derived factor as a multifunctional regulator of wound healing. *Am. J. Physiol. Circ. Physiol.* **309**, H812–H826 (2015).
52. Saito, Y., Chikenji, T. S., Matsumura, T., Nakano, M. & Fujimiya, M. Exercise enhances skeletal muscle regeneration by promoting senescence in fibro-adipogenic progenitors. *Nat. Commun.* **11**, 889 (2020).
53. Chikenji, T. S. *et al.* p16INK4A-expressing mesenchymal stromal cells restore the senescence–clearance–regeneration sequence that is impaired in chronic muscle inflammation. *EBioMedicine* **44**, 86–97 (2019).
54. Svensson, P.-A. *et al.* CDKN2B expression and subcutaneous adipose tissue expandability: Possible influence of the 9p21 atherosclerosis locus. *Biochem. Biophys. Res. Commun.* **446**, 1126–1131 (2014).
55. Hernandez-Segura, A., Nehme, J. & Demaria, M. Hallmarks of Cellular Senescence. *Trends Cell Biol.* **28**, 436–453 (2018).
56. Zhang, Y., Alexander, P. B. & Wang, X.-F. TGF-β Family Signaling in the Control of Cell Proliferation and Survival. *Cold Spring Harb. Perspect. Biol.* **9**, (2017).
57. Staller, P. *et al.* Repression of p15INK4b expression by Myc through association with Miz-1. *Nat. Cell Biol.* **3**, (2001).
58. Chen, C.-R., Kang, Y. & Massague, J. Defective repression of c-myc in breast cancer cells: A loss at the core of the transforming growth factor growth arrest program. *Proc. Natl. Acad. Sci.* **98**, (2001).
59. Battegay, E. J., Raines, E. W., Seifert, R. A., Bowen-Pope, D. F. & Ross, R. TGF-β induces bimodal proliferation of connective tissue cells via complex control of an autocrine PDGF loop. *Cell* **63**, (1990).
60. Morikawa, M., Derynck, R. & Miyazono, K. TGF-β and the TGF-β Family: Context-Dependent Roles in Cell and Tissue Physiology. *Cold Spring Harb. Perspect. Biol.* **8**, (2016).
61. Smina, T. P., Rabeka, M. & Viswanathan, V. Diabetic Foot Ulcer as a Cause of Significant Decline in the Renal Function Among South Indian Population With Type 2 Diabetes: Role of TGF-β1 and CCN Family Proteins. *Int. J. Low. Extrem. Wounds* **18**, (2019).
62. Driskell, R. R., Jahoda, C. A. B., Chuong, C.-M., Watt, F. M. & Horsley, V. Defining dermal adipose tissue. *Exp. Dermatol.* **23**, 629–631 (2014).
63. Chen, S. X., Zhang, L.-J. & Gallo, R. L. Dermal White Adipose Tissue: A Newly Recognized Layer of Skin Innate Defense. *J. Invest. Dermatol.* **139**, 1002–1009 (2019).
64. Sun, C. *et al.* Mosaic Mutant Analysis Identifies PDGFRα/PDGFRβ as Negative Regulators of Adipogenesis. *Cell Stem Cell* **26**, (2020).
65. Ansell, D. M., Holden, K. A. & Hardman, M. J. Animal models of wound repair: Are they cutting it? *Exp. Dermatol.* **21**, (2012).

66. Bing, C. & Trayhurn, P. New insights into adipose tissue atrophy in cancer cachexia. *Proc. Nutr. Soc.* **68**, 385–392 (2009).
67. Alves, M. J. *et al.* Adipose tissue fibrosis in human cancer cachexia: the role of TGFβ pathway. *BMC Cancer* **17**, (2017).
68. Gunawardana, S. C. Adipose Tissue, Hormones, and Treatment of Type 1 Diabetes. *Curr. Diab. Rep.* **12**, 542–550 (2012).
69. KAWAI, S., TAKAGI, Y., KANEKO, S. & KUROSAWA, T. Effect of Three Types of Mixed Anesthetic Agents Alternate to Ketamine in Mice. *Exp. Anim.* **60**, 481–487 (2011).
70. Kanda, Y. Investigation of the freely available easy-to-use software 'EZR' for medical statistics. *Bone Marrow Transplant.* **48**, 452–458 (2013).

Table

Table 1: Patient Demographics

Donor/Group	Sex	Age	DM Daignosis	HbA1c (NGSP) [%]	Diagnosis	Region	Days post wound	Comorbidity	Medication
Non-DM1	Male	65	-	-	Electoric injury, Burn	Abdomen	19	Postoperative liver cancer	
Non-DM2	Male	82	-	-	Burn	Thigh	39	Chronic renal impairment, myocardial infarction, cerebral infarction, dementia, postoperative colorectal cancer	Aspirin, Carvedilol, Amlodipine besilate, Amiodarone hydrochloride, Silodosin, Esomeprazole magnesium hydrate, Acetaminophen
Non-DM3	Male	65	-	-	Burn	Lower leg	39	Hypertension, hypercholesteremia, narcolepsy	Aspirin, Carvedilol, Clopidogrel sulfate, Vitamin B6, Vitamin B12, Ramelteon, Suvorexant, someprazole magnesium hydrate, Loxoprofen sodium hydrate, Amoxicillin hydrate
Non-DM4	Male	45	-	-	Burn	Hip	39	Traumatic intracranial hemorrhage	
Non-DM5	Female	70	-	-	Pressure ulcer	Chest	70	COPD, mammary cancer	Fluticasone Furoate, Umeclidinium bromide vilanterol trifenatate, Cilnidipine, Allopurinol, Sodium risedronate hydrat, Rabeprazole sodium, Domperidone, Kampo medicien
Non-DM6	Male	21	-	-	Paraplegia, Pressure ulcer	Ischial region	84	Spinal cord injury	
DM1	Female	76	+	7.1	Chronic traumatic ulcer	Elbow	11	Thrombocytopenic purpra, atrial fibrillation, iron deficiency anemia, dementia, Stomach cancer, bone lesions	Denosumab, Prednisolone (15mg/day), Fenofibrate, Pilsicainide hydrochloride hydrate, Vonoprazan fumarate, Clotiazepam, Solifenacin succinate, Sodium Ferrous Citrate,
DM2	Male	64	+	7.3	Burn	Thigh	13	Hypertension	unknown
DM3	Male	60	+	5.2	Burn	Back	17	Hepatic encephalopathy, liver cancer, liver cirrhosis, esophagealn varices	Apixaban, Furosemide, Azilsartan, Spironolactone, Verapamil hydrochloride, Entecavir hydrate, Sorafenib Tosilate, Monoammonium glycyrrhizinate glycine aminoacetic acid DL-methionine, Rifaximin, Vonoprazan fumarate, Tramadol hydrochloride acetaminophen, Dried ferrous sulfate
DM4*	Male	60	+	5.2	Burn	Abdomen	31	Hepatic encephalopathy, liver cancer, liver cirrhosis, esophagealn varices	Apixaban, Furosemide, Azilsartan, Spironolactone, Verapamil hydrochloride, Entecavir hydrate, Sorafenib Tosilate, Monoammonium glycyrrhizinate glycine aminoacetic acid DL-methionine, Rifaximin, Vonoprazan fumarate, Tramadol hydrochloride acetaminophen, Dried ferrous sulfate
DM5	Male	70	+	11	Fournier Gangrene	Hip	35	Hypercholesteremia	Metformin hydrochloride, Glimepiride, Liraglutide, Insulin degludec, Liraglutide, Olmesartan medoxomil, Canagliflozin hydrate, Pitavastatin calcium hydrate, Nizatidine
DM6	Female	82	+	6.3	Ulcer after vein graft harvest	Lower leg	64	Aortic stenosis, postoperative abdominal aortic aneurysm, interstitial lung disease, hypercholesteremia, inflammation of mesentric adipose tissue, ischemic enteritis, cholangitis	Vildagliptin, Insulin lispro, Insulin glargine, Atorvastatin calcium hydrate, Ethyl icosapentate, Telmisartan, Bisoprolol fumarate, Furosemide, Amlodipine besilate, sennoside A,B, Levocetirizine hydrochloride

*Same patient as DM3

Figures

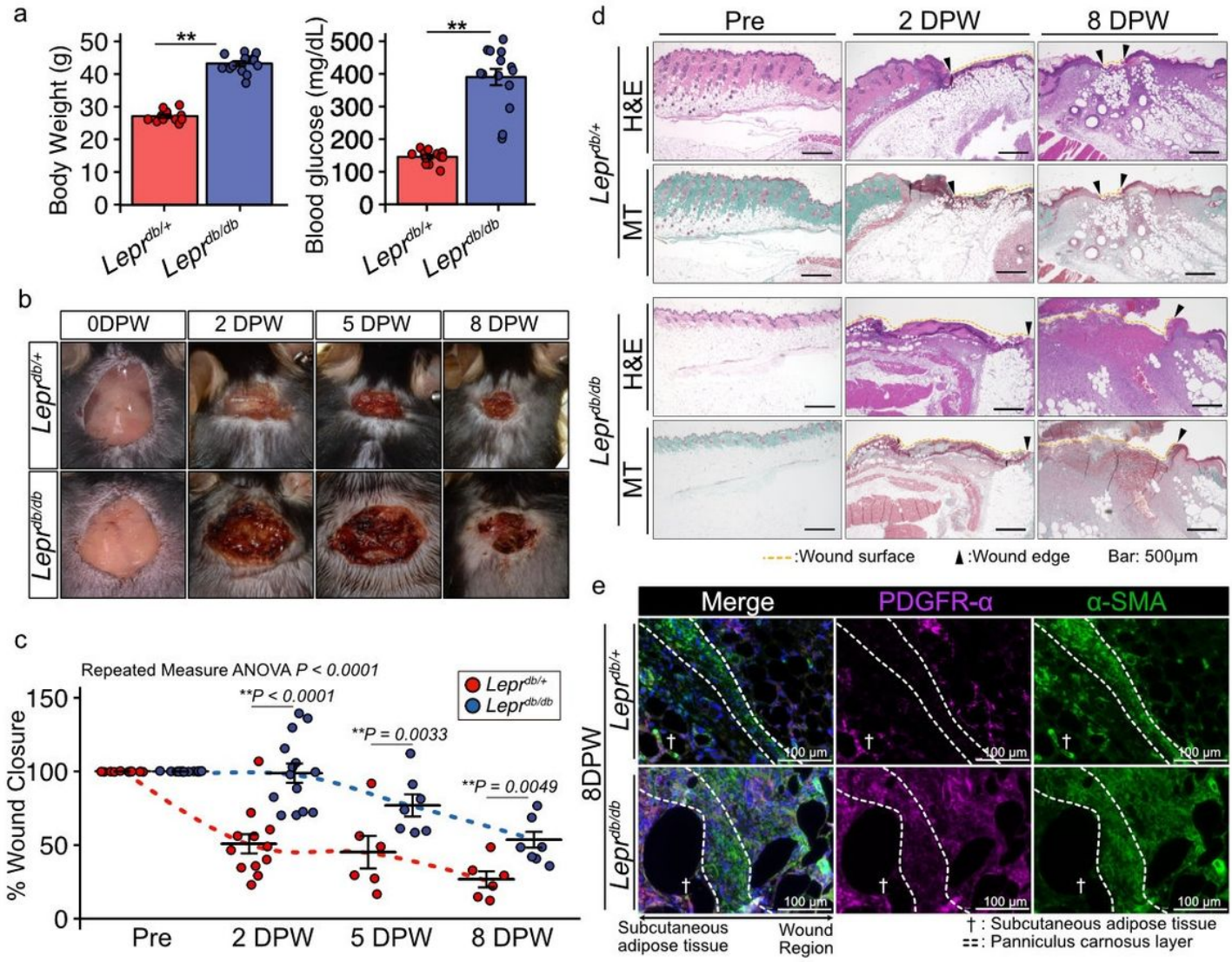

Figure 1

Leprdb/db mice exhibit impaired wound healing (a) Body weight and blood glucose levels for Leprdb/+ and Lperdb/db mice before full-thickness excisional skin wounds were created (n=12 for Leprdb/+ and n=14 for Lperdb/db mice). (b) Representative wound images during the healing process and (c) the wound area, reported as the percent of wound closure compared to the 0 days post wound (0 DPW) area (n=12¬–14 for 0 DPW and 2 DPW and n=6–7 for 5 DPW and 8 DPW). (d) Representative image of H&E staining and Masson trichrome (MT) staining of a wound at pre-wound, 2 DPW, and 8 DPW. (e) Representative images of PDGFR-α and α-SMA immunostaining of a wound at 8 DPW. Quantitative data are shown as means±SE in dot plots. p-values were determined using a two-tailed Student's t-test or one-way ANOVA adjusted by the Tukey method (*p<0.05 and **p<0.001).

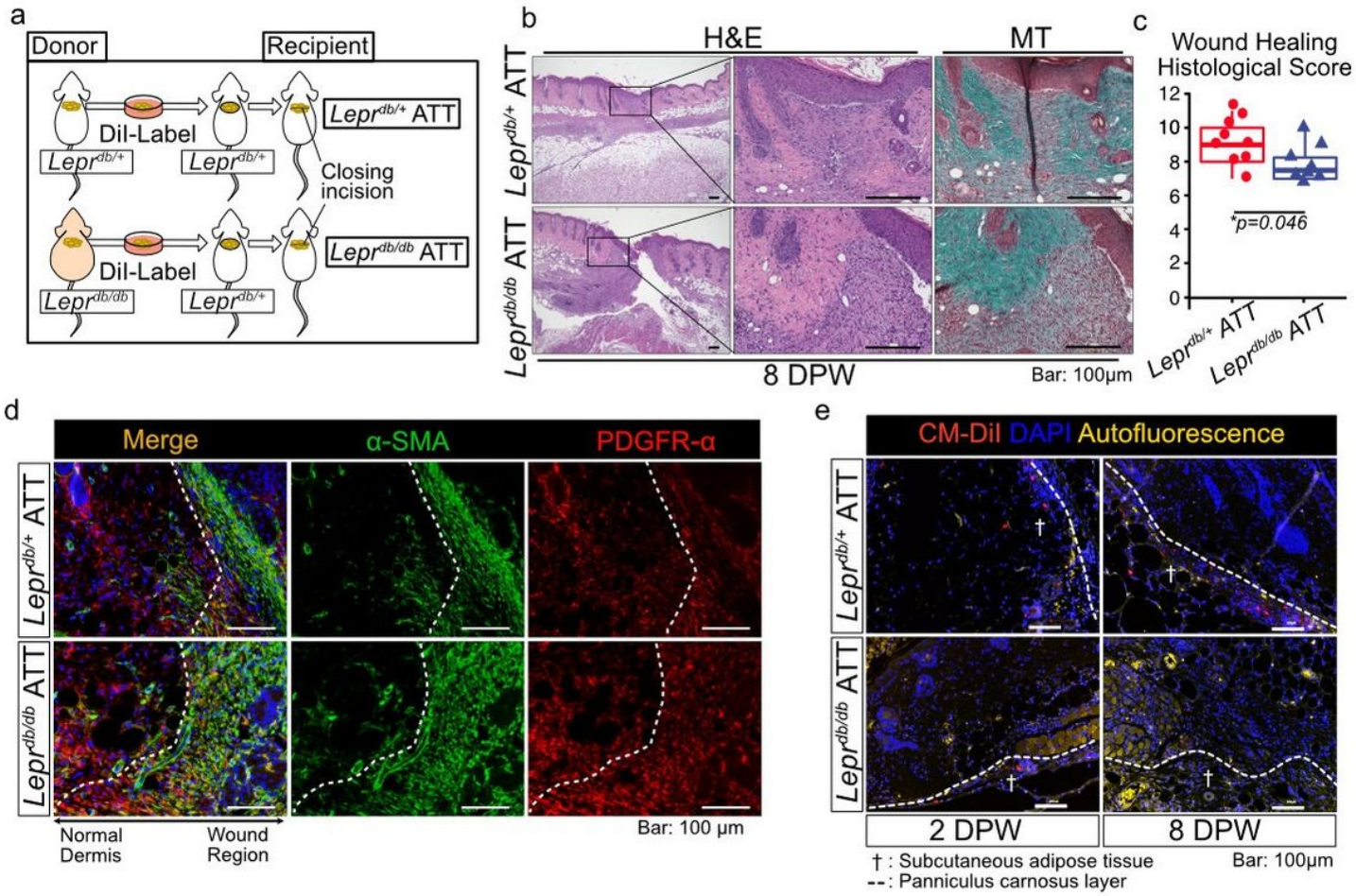

Figure 2

Transplantation of adipose tissue derived from Leprdb/db mice into Leprdb/+ mice impairs wound healing (a) Schematic diagram of the procedure for the adipose tissue transplantation (ATT) experiments. (b) Representative image of H&E staining and MT staining of a wound at 8 DPW and (c) the quantitative analysis of the wound healing histological score (n=8 for each group). (d) Representative images of PDGFR-α and α-SMA immunostaining of a wound edge at 8 DPW. (e) Localization of CM-DiI–labeled adipose tissue–derived cells in wound regions. Quantitative data are shown as medians with IQRs and 1.5 times the IQR and are displayed as box-and-whisker plots. p-values were determined using a two-tailed Student's t-test (*p<0.05).

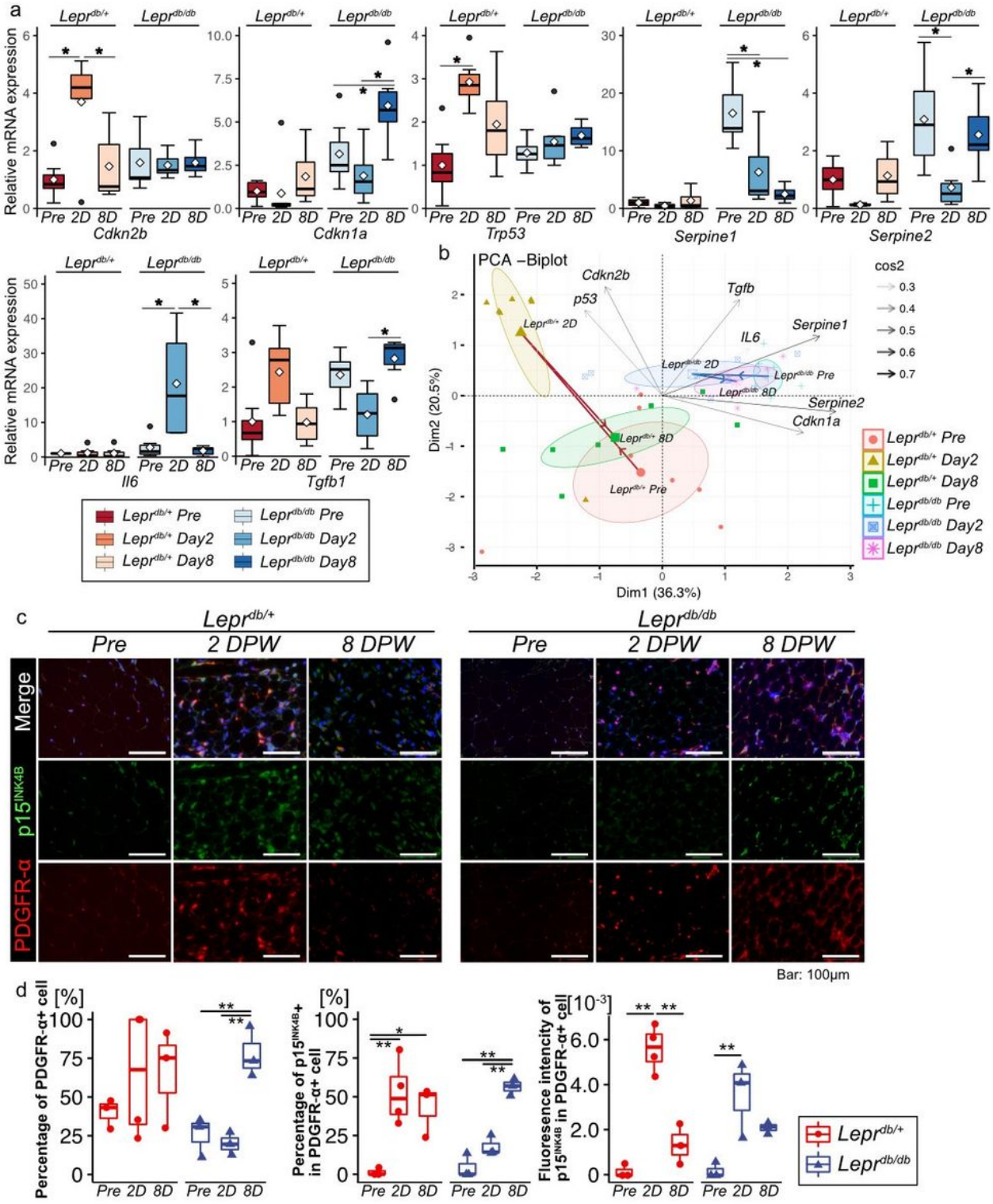

Figure 3

Cellular senescence in subcutaneous adipose tissue during wound healing in Leprdb/+ and Leprdb/db mice (a) Relative mRNA expression of senescence-related genes at pre-wound, 2 DPW, and 8 DPW in Leprdb/+ and Leprdb/db mice (n=6¬–7 for each group) and (b) principal component analysis (PCA) of the levels of senescence for senescence-related genes at pre-wound, 2 DPW, and 8 DPW for Leprdb/+ and Leprdb/db mice. (c) Representative images of PDGFR-α and p15INK4B immunostaining of adipose tissue

at pre-wound, 2 DPW, and 8 DPW and (d) quantitative data for the percentage of PDGFR-α– and p15INK4B–positive cells and the fluorescence intensity of p15INK4B in PDGFR-α–positive cells (n=3¬–4 for each group). Quantitative data are presented as the means and medians with IQRs and 1.5 times the IQR and are displayed as box-and-whisker plots. p-values were determined using one-way ANOVA adjusted by the Tukey method (*p<0.05 and **p<0.001).

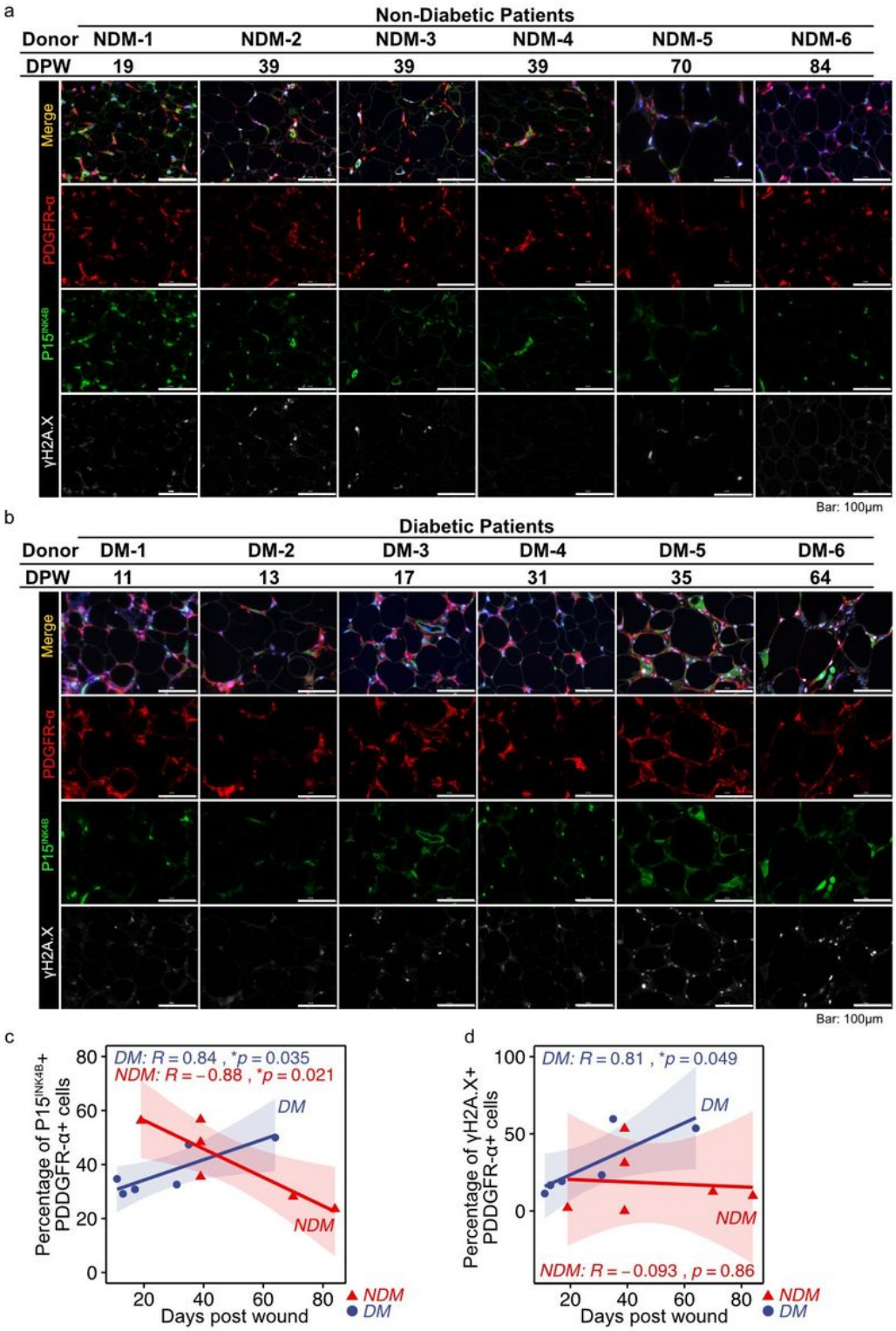

Figure 4

Cellular senescence in subcutaneous adipose tissue during wound healing in diabetic patients (a–b) Representative images of PDGFR-α, p15INK4B, and γH2A.X immunostaining of adipose tissue during wound healing in diabetic or non-diabetic patients. (c–d) Correlation between the percentage of p15INK4B– or γH2A.X–positive cells in PDGFR-α–positive cells and the time post-wound (n=6 for each group). Correlations were examined statistically using Pearson's correlation coefficient, and 95% confidence intervals are shown with translucent fill corresponding to each marker color.

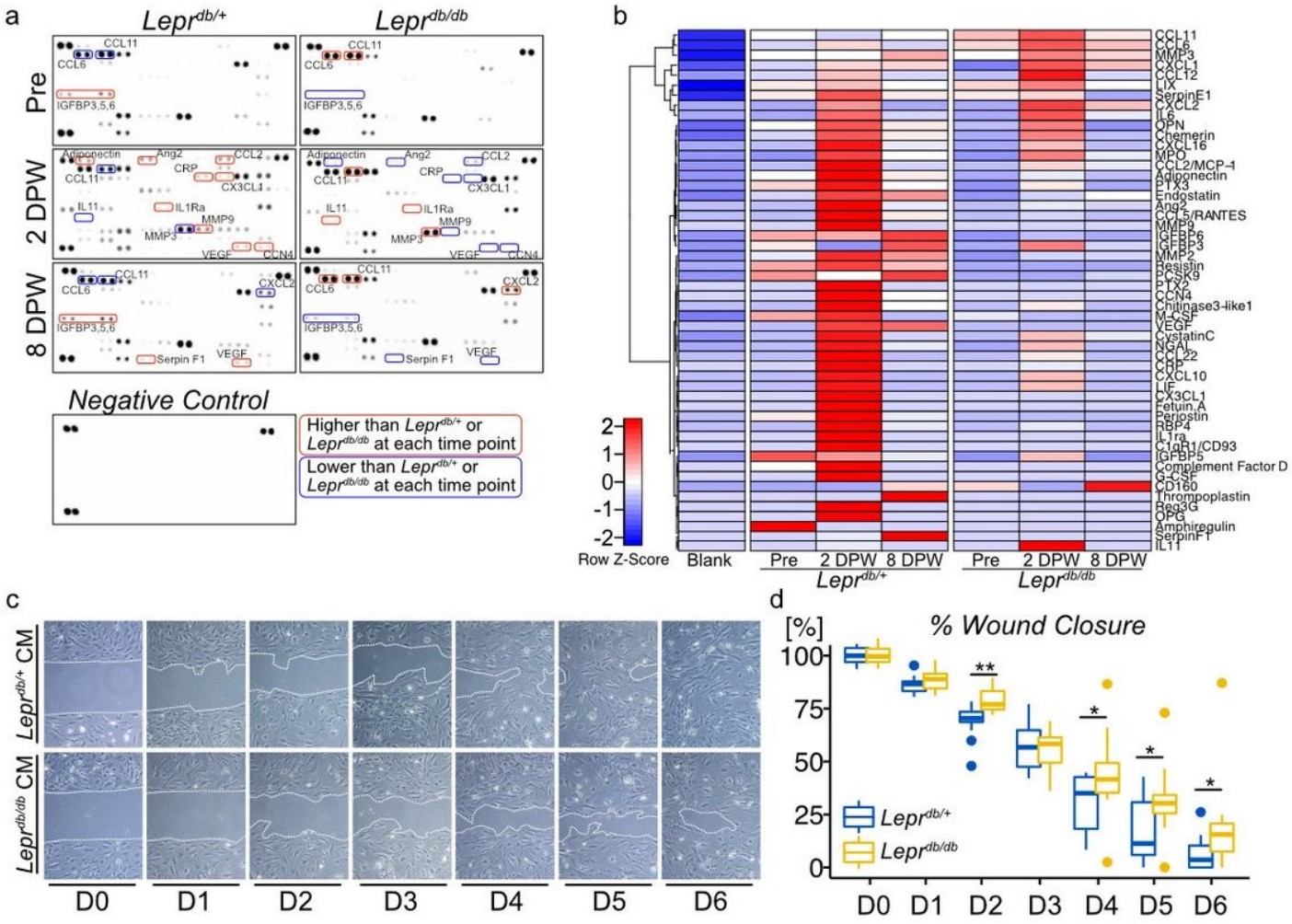

Figure 5

Components of post-wound adipose tissue–derived cytokines in Leprdb/+ and Leprdbdb+ mice and their effect on cell migration (a) Proteome profiler antibody array analysis of SASP-containing culture media collected from the organ culture of adipose tissue at pre-wound, 2 DPW, and 8 DPW. (b) Hierarchical clustering of differentially expressed cytokine expression. Cytokines with higher expression are depicted in red, cytokines with lower expression are depicted in blue, and cytokines with no difference are depicted in white. (c) Representative phase-contrast image of scratch assay treated with Leprdb/+ or Leprdb/db adipose tissue–derived cultured media and (d) the percentage of wound closure at each time point, from immediately after wound creation (D0) to 6 days after wound (D6) (n=5 for each group). Quantitative

data are shown as medians with IQRs and 1.5 times the IQR and are displayed as box-and-whisker plots. p-values were determined using one-way ANOVA adjusted by the Tukey method (*p<0.05 and **p<0.001).

Supplementary Files

This is a list of supplementary files associated with this preprint. Click to download.

- SupplFigureKitaFinal.docx
- nrreportingsummarykita.pdf